



## EFFECTS OF THE YUFUTSU BASIN ON STRUCTURAL RESPONSE DURING SUBDUCTION EARTHQUAKES

N.A. Marafi<sup>(1)</sup>, M.O. Eberhard<sup>(2)</sup>, J.W. Berman<sup>(3)</sup>

<sup>(1)</sup> Graduate Research Assistant, Department of Civil and Environmental Engineering, University of Washington, marafi@uw.edu

<sup>(2)</sup> Professor, Department of Civil and Environmental Engineering, University of Washington, eberhard@uw.edu

<sup>(3)</sup> Associate Professor, Department of Civil and Environmental Engineering, University of Washington, jwberman@uw.edu

### **Abstract**

Sedimentary basins tend to increase the intensity of ground-motions and the resulting damage to structures. Although current U.S. seismic hazard maps do not account for the effects of basins, most ground-motion prediction equations for crustal earthquakes include basin amplification terms, which amplify spectral acceleration at long periods. For most subduction earthquake GMPEs, these basin terms have not yet been developed. In addition, none of the available GMPEs account for the effects of basins on ground-motion duration and spectral shape. These omissions are particularly important in the Pacific Northwest of the United States, because this region has several deep basins, and even without considering basin effects, subduction earthquakes contribute a large portion of the overall seismic hazard, particularly at long periods. This paper quantifies the effects of the Yufutsu basin in Japan, which is similar to the deep basin underlying the Seattle region.

For several subduction earthquakes of varying magnitude, the effects of basins are evaluated by comparing ground-motion recordings from stations located inside and near the Yufutsu basin. Basin effects are quantified using spectral acceleration, significant duration, and a new ductility dependent spectral shape intensity measure,  $SS_a$ . The results of collapse analyses are reported for a set of well-studied archetypical building frame models, for which the ground-motion intensity at collapse is explained in terms of the three intensity measures. Finally, design strength amplification factors are developed with the aim of achieving collapse margin ratio for structures located inside basins during subduction earthquakes that are similar to those achieved by conventional structural designs.

*Keywords: sedimentary basins, spectral acceleration, duration, spectral shape, structural collapse*

## 1 Introduction

Sedimentary basins are known to increase the intensity of ground motions [e.g., 1, 2, 3, 4]. These amplifications are generally attributed to: (1) impedance contrasts between basin layers, (2) focusing of shear-waves at the surface, and (3) conversion of shear-waves into surface waves at the basin edges [5]. The basin amplification phenomenon is consistent with the increased levels of damage observed within basins during earthquakes, including the 1994 Northridge [2], the 1995 Kobe [1], the 2001 Nisqually [4], and Tokachi-Oki [3, 6] earthquakes. Several deep basins are located in the Pacific Northwest of the United States.

Subduction earthquakes are particularly important in the Pacific Northwest (PNW), because they have large contributions to the hazard, particularly for long periods. For example, in downtown Seattle, subduction interface earthquakes contribute 47% of the total hazard for the 2.0-s spectral acceleration corresponding to the Maximum Considered Earthquake (mean return time of 2475 years) [7]. Subduction intraslab earthquake contribute another 22%. In addition, the GMPEs used to generate the seismic hazard maps do not account for the effects of basins on ground-motion duration and spectral shape, which also affect structural response [8, 9, 10, 11, 12].

This paper characterizes the effects of the Yufutsu basin in Hokaido, Japan on the measured spectral accelerations, ground-motion durations, and spectral shapes for motions measured during subduction earthquakes. The paper focuses on this basin, because it is similar to that underlying the Puget Sound region, including Seattle. To evaluate this effect, ground-motion recordings from inside and outside the basin are compared for a series of earthquakes. The effects of basins on structural collapse are quantified using an incremental dynamic analysis of 30 archetypical building frame models [13]. The collapse fragilities for inside and outside basin motions are compared and design strength amplification factors are computed to achieve collapse margin ratios similar to those in conventional structural designs.

## 2 Existing Treatment of Basin Effects within GMPEs

Current US National Seismic Hazard Maps [14, 15] do not account for the effects of basins on spectral acceleration. However, several recently developed ground-motion prediction equations (GMPEs) for crustal earthquakes take into account the effects of basins on spectral accelerations [16, 17, 18, 19]. In contrast, the influence of basins is not incorporated in most GMPEs [20, 21, 22, 23] for interface and intraplate subduction earthquakes. These earthquake sources often dominate the PNW seismic hazard at long periods where current GMPE basin amplifications are particularly large.

GMPEs usually account for the increase in spectral acceleration with basin depth in terms of the depth at which a particular shear-wave velocity ( $V_s$ ) is measured. The threshold shear-wave velocity varies among GMPEs [16, 17, 18, 19, 24]. This paper characterizes basin depth in terms  $Z_{2.5}$ , which corresponds to the depth to a shear-wave velocity ( $V_s$ ) of 2.5 km/s. This relatively high velocity is a better indicator of basin depth than lower velocities for deep basins such as the Puget Lowland basin because most of the Puget Sound region has a thick layer of glacial till with a  $V_s$  around 1 km/s [25]. In addition, Campbell and Bozorgnia use  $Z_{2.5}$  for their GMPE [19], referred in this paper as CB14. Figure 1 shows the variation of the GMPE amplification factor with respect to the fundamental period of structure ( $T_n$ ) for representative values of  $Z_{2.5}$ . For shallow basins (e.g.,  $Z_{2.5}=0.5$  km), the factor is larger than 1 at short periods and is less than 1 at longer periods.  $S_a$  values are unchanged for values of  $Z_{2.5}$  between 1 and 3. The amplification factor reaches a maximum value of 1.3 for  $Z_{2.5} = 4.5$  km and 1.6 for  $Z_{2.5} = 6$  km. Both maxima occur at a period of 7.5 seconds.

GMPEs do not characterize other ground motion characteristics that correlate with structural damage. Bommer et al. [8], and Hancock and Bommer [9] have shown that duration influences engineering demand measures. Chandramohan et al. [10], and Raghunandan and Liel [11] found that the ground-motion's duration can affect the minimum design strength needed to avoid collapse. Similarly, Haselton et al. [26], Eads et al. [27], and Marafi et al. [12] have shown that spectral shape influences the collapse probabilities of structures.

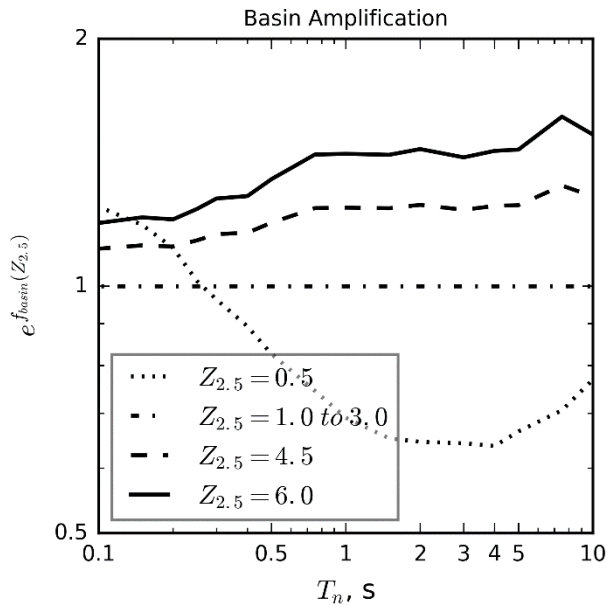


Figure 1.  $Z_{2.5}$  basin amplification factor from the Campbell and Bozorgnia GMPE [19]

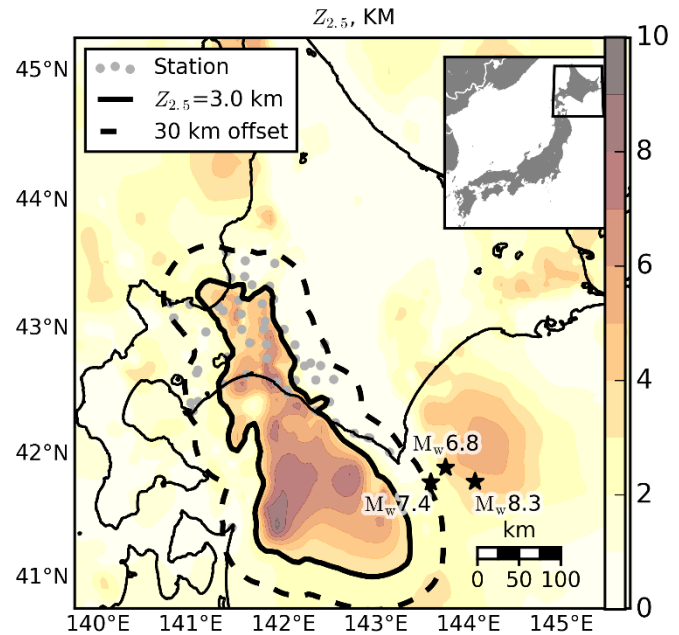


Figure 2.  $Z_{2.5}$  map of Hokkaido, Japan showing the Yufutsu basin along with epicenters of three subduction earthquakes.

### 3 Seismic Stations in and near Yufutsu Basin

The Yufutsu basin is of special interest, because it has been subjected to subduction earthquakes (e.g. 2003 Tokachi-Oki), and its depth is similar to that of the Puget Lowland basin. Figure 2 shows the Yufutsu basin, characterized in terms of the basin depth parameter,  $Z_{2.5}$ , as extracted from the Japan Integrated Velocity Structure Model [28]. The Yufutsu basin, which is partly underwater, has  $Z_{2.5}$  values reaching near 8 km onshore. The Puget Lowland Basin has values of  $Z_{2.5}$  ranging up to 8km too [29].

Ground motions near and inside the Yufutsu basin have been recorded by the Kik-Net and K-NET seismic networks [30]. To reduce the effects of soft-soil amplification, this paper considers only onshore surface recordings from stations with average shear-wave velocity in the upper 30 meters,  $V_{S30}$ , that exceed 180 m/s, which corresponds to the site class D/E boundary. The values of  $V_{S30}$  were computed from the soil profile data available on the K-NET/Kik-Net database [30]. K-Net station soil profiles do not extend down to 30m, so values of  $V_{S30}$  were computed following the recommendations of Boore et al. [31].

As reported in Table 1, about 20 stations have values of  $Z_{2.5}$  of at least 3km, and there are about 35 stations located near the basin, but for which  $Z_{2.5}$  is less than 3km. Stations were designated as being “near” the basin if they were located within 30 km of the  $Z_{2.5}=3$ km contour line. For all of the stations, the closest distance to rupture ( $R_{CD}$ ) was less than 250 km ( $R_{CD}$  was taken from [32]). For each event (three are shown), the median source-to-site distance (either  $R_{hyp}$  or  $R_{CD}$ ) is similar for each  $Z_{2.5}$  bin. However, the log-normal standard deviations for distance is larger for smaller values of  $Z_{2.5}$ , as expected, because they surround the basin edge.

Table 1. Yufutsu basin station recordings for each  $Z_{2.5}$  bin

Eq.	$M_w$	Depth	$Z_{2.5} < 1.5$			$1.5 \leq Z_{2.5} < 3.0$			$3.0 \leq Z_{2.5} < 4.5$			$4.5 \leq Z_{2.5}$						
			#	$\bar{R}^1$	$\sigma_{tn}$	$\bar{Z}_{2.5}$	#	$\bar{R}^1$	$\sigma_{tn}$	$\bar{Z}_{2.5}$	#	$\bar{R}^1$	$\sigma_{tn}$	$\bar{Z}_{2.5}$	#	$\bar{R}^1$	$\sigma_{tn}$	$\bar{Z}_{2.5}$
Tokachi-Oki <sup>a</sup>	8.3	27	21	125	0.49	0.39	15	143	0.33	2.03	8	139	0.34	3.51	12	136	0.16	5.46
Hokkaido <sup>b</sup>	7.4	41.8	21	173	0.45	0.35	14	201	0.25	2.06	8	203	0.26	3.51	11	203	0.12	5.29
Hokkaido <sup>b</sup>	6.8	41.9	21	156	0.5	0.4	15	189	0.27	2.03	8	189	0.28	3.51	12	184	0.13	5.46

Notes: <sup>1</sup>Closest distance to Rupture ( $R_{CD}$ ) is used for interface events and hypocentral distances ( $R_{hyp}$ ) is used for intra-slab events.

BC-Hydro GMPE event terms: <sup>a</sup>interface, <sup>b</sup>intraslab

## 4 Effects of Basin on Spectral Acceleration

In structural design, the earthquake loads are usually computed from a design spectral acceleration at the fundamental period of the structure. Figure 3 shows the median  $S_a$  ( $\tilde{S}_a$ ) with respect to period for each  $Z_{2.5}$  bin for the Tokachi-Oki earthquake.  $\tilde{S}_a$  consistently increases with  $Z_{2.5}$  for all bins, but the ratio of  $\tilde{S}_a$  between bins varies with period. For example, the ratio of  $\tilde{S}_a$  at 0.5s is  $\approx 2$  between the shallowest and deepest  $Z_{2.5}$  bins, whereas this ratio increases to  $\approx 3$  at 5 seconds.

### 4.1 Relating GMPE Residuals to $Z_{2.5}$

It is not sufficient to look at variations of  $S_a$  between stations, because recordings also vary due to site-to-source attenuation and local site properties. These variations can be accounted by normalizing the measured accelerations by those expected from GMPEs that do not account for basins.

GMPEs include a series of terms that account for a variety of properties that correlate to ground-motion intensity measures. The natural-log of spectral acceleration at several periods is a commonly predicted IM and usually has the following form:

$$\ln S_{a,GMPE} = f_{M,R}(M, R) + f_{site}(\dots) + f_{basin}(\dots) + \epsilon \quad \text{Eq. 1}$$

where  $f_{M,R}$  is the term that accounts for the effects associated with magnitude ( $M$ ) and source-to-site distance ( $R$ ).  $f_{site}$  accounts for local site effects, such as  $V_{S30}$ . In some GMPEs,  $f_{basin}$  exists and incorporates the effects due to sedimentary basins.  $\epsilon$  is the residual due to parameters not accounted for in the GMPE.

The GMPE residuals provide a convenient way of identifying the effects of basins on  $S_a$ . The GMPE residual is computed as the difference between the log-natural of the recorded  $S_a$  and the log-natural of the predicted  $S_a$ . The residual is computed as,

$$\epsilon = \ln S_{a,rec.} - \ln S_{a,GMPE} = \epsilon_{basin}(\dots) + \epsilon_{other}(\dots) \quad \text{Eq. 2}$$

where  $\epsilon_{basin}$  is the residual due to sedimentary basin effects not included in the GMPE, and  $\epsilon_{other}$  is the residual due to other effects not captured by the GMPE. In this paper, the mean residual for all the recordings in a particular bin is denoted as  $\bar{\epsilon}_Z$ . The difference in mean residual between a particular bin to the shallowest bin ( $Z_{2.5} < 1.5$ ) is denoted as  $\Delta\bar{\epsilon}_Z$  and expressed as,

$$\Delta\bar{\epsilon}_Z = \bar{\epsilon}_Z - \bar{\epsilon}_{Z < 1.5} = [\bar{\epsilon}_{Z,basin} + \bar{\epsilon}_{Z,other}] - [\bar{\epsilon}_{Z < 1.5,basin} + \bar{\epsilon}_{Z < 1.5,other}] \quad \text{Eq. 3}$$

where  $\bar{\epsilon}_{Z < 1.5}$  is defined as the mean residual for recordings with  $Z_{2.5} < 1.5$ . Assuming that the GMPE residuals due to non-basin effects are the same inside and outside the basin,  $\Delta\bar{\epsilon}$  can be approximated as,

$$\Delta \bar{\epsilon}_Z \approx \bar{\epsilon}_{Z,basin} - \bar{\epsilon}_{Z<1.5,basin} \quad \text{Eq. 4}$$

In this paper, the basin amplification factor,  $BAF_{S_a}$ , is defined as the exponential of  $\Delta \bar{\epsilon}_Z$ .

$$BAF_{S_a}(Z) = e^{\Delta \bar{\epsilon}_Z} = \exp \frac{\bar{\epsilon}_Z}{\bar{\epsilon}_{Z<1.5}} = \frac{\left( \prod_{y=1}^Y \frac{S_{a,Z}^y}{S_{a,Z,GMPPE}^y} \right)^{\frac{1}{Y}}}{\left( \prod_{x=1}^X \frac{S_{a,Z}^x}{S_{a,Z,GMPPE}^x} \right)^{\frac{1}{X}}} \quad \text{Eq. 5}$$

where  $X$  is the number of ground-motions with  $Z_{2.5} < 1.5$  and  $Y$  is the number of ground-motion within a particular  $Z_{2.5}$  range.  $BAF_{S_a}$  can be interpreted as the geometric mean of the ratio of the measured to predicted spectral accelerations inside basin  $S_a$ , normalized by the same quantify outside the basin.

Several subduction GMPE are used in the U.S. hazard maps. This paper focuses on the most recently developed one, the BC-Hydro GMPE [33], published in 2016. The BC-Hydro [33] GMPE uses terms that distinguish between stations located in the forearc (between the subduction trench and the volcanic fronts) and the backarc region (beyond the volcanic fronts). Stations used in the Yufutsu basin are assumed to be located in the backarc. Figure 4 shows values of  $BAF_{S_a}$  computed for  $Z_{2.5}$  ranges of: 1.5-3km, 3-4.5km, and  $Z_{2.5} > 4.5$ km. The  $BAF_{S_a}$  values exceed one for all three bins and for all periods.  $BAF_{S_a}$  generally increases with basin depth and  $Z_{2.5}$ , reaching maximum values between 3 and 4 at long periods (5-7s).

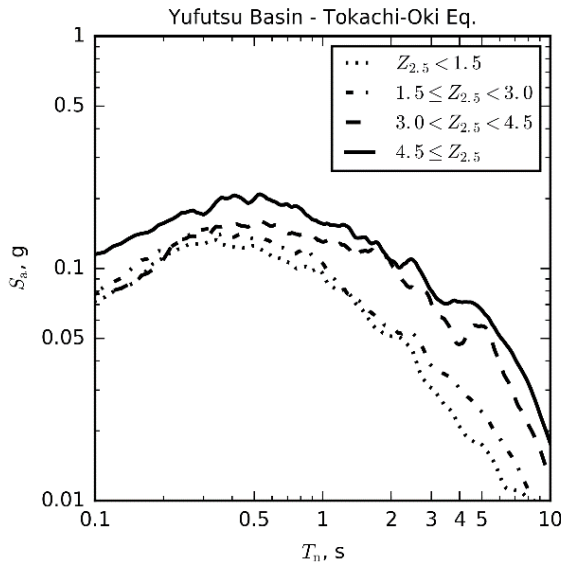


Figure 3. Median  $S_a$  with respect to the fundamental period of structure for recordings binned in terms of  $Z_{2.5}$  ranges.

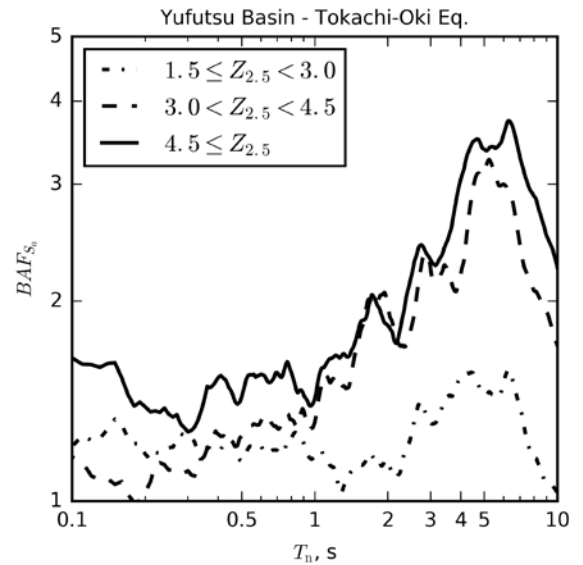


Figure 4. Basin Amplification Factors with respect to the fundamental period of structure for varying  $Z_{2.5}$  ranges.

## 4.2 Effect of Magnitude

For crustal earthquakes, GMPE basin terms [16, 17, 18, 19, 24] are independent of earthquake magnitude. To evaluate the effects of magnitude for subduction earthquakes, Figure 5 compares  $BAF_{S_a}$  values computed for Tokachi-Oki ( $M_w$  8.3) with those computed for two lower-magnitude events ( $M_w$  7.4 and 6.8). These lower magnitude events occur at depths larger than 40 km (shown in Table 1), and they have similar source-to-site distances. Both lower-magnitude events are assumed to be intraslab events in the BC-Hydro GMPE predictions.

Figure 5 compares the  $BAF_{S_a}$  for the three earthquakes. To facilitate the comparison, a single bin is considered for each event, in which the  $BAF_{S_a}$  values are computed for recordings from stations that have  $Z_{2.5} \geq$

3 km. The number of recordings are similar between events (Table 1). The  $BAF_{Sa}$  shown in Figure 5 have similar magnitudes and trends with respect to period.

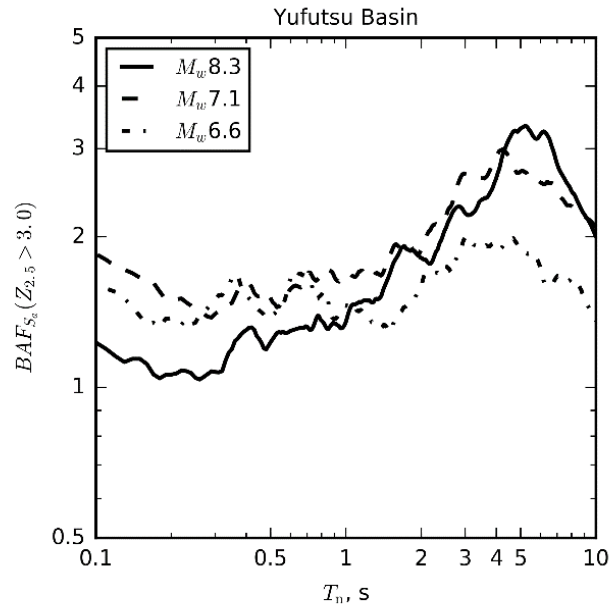


Figure 5.  $BAF_{Sa}$  with respect to the fundamental period of the structure for varying magnitude earthquakes.

## 5 Effects of Basin on Significant Duration

Bommer et al. [8] found that the effects of durations are pronounced in structures that are susceptible to low-cycle fatigue and undergo strength and stiffness degradation with dynamic loading. Hancock and Bommer [9], and Chandramohan et al. [10] predicted structural response with various duration IMs. Chandramohan et al. [10] found that  $D_s$  was most suitable and correlates well with structural collapse capacity as computed with nonlinear dynamic analysis. This paper characterizes ground-motion duration using significant duration, and is defined as the time between two target values of the integral,  $\int_0^{t_{max}} a_g(t)^2 dt$ , where  $a_g$  is the ground acceleration, and  $t_{max}$  is the total duration of the record. This paper uses significant duration computed at the 5-95% threshold,  $D_{s,5-95\%}$ .

Significant durations were computed for all the stations listed in Table 1. The effects of basin on duration can be seen in Figure 6, which shows  $D_{s,5-95\%}$  with respect to  $Z_{2.5}$ . Figure 6 also shows the results of a simple linear regression analysis. The resulting p-value of 0.01 is less than the value of 0.05 conventionally used as a threshold to reject the null hypothesis. However, the low of  $R^2 = 0.11$  indicates that this relationship is not strong. Several duration GMPEs [34, 35, 36] have recognized that significant duration increases with distance, however accounting for this effect using GMPE residuals did not lead to improved correlations.

## 6 Effects on Basin on Spectral Shape

Haselton et al. [26] and Eads et al. [27], among others, have shown that spectral shape influences collapse probabilities for structures. Marafi et al. [12] developed a spectral shape intensity measure,  $SS_a$ , that accounts for the differences in period elongation between brittle and ductile structures. To assess effects of the basins spectral shape,  $SS_a$  is related to  $Z_{2.5}$ .

$SS_a$  is defined using the integral of the ground-motion response spectrum (damping ratio of 5%) between the fundamental period of the building ( $T_n$ ) and the nominal elongated period ( $\alpha T_n$ ). To make  $SS_a$  independent

of the ground-motion amplitude, the integral is then normalized by the area of a rectangle with a height of  $S_a(T_n)$  and width of  $(\alpha-1)T_n$ .

$$SS_a(T_n, \alpha) = \frac{\int_{T_n}^{\alpha T_n} S_a(T) dT}{S_a(T_n)(\alpha-1)T_n} \quad \text{Eq. 6}$$

where  $\alpha T_n$  is computed as a multiple of the secant stiffness of the structure at maximum displacement resulting in  $\alpha = C_\alpha \sqrt{\mu}$  where  $C_\alpha$  is optimized as 1.3 in [12], and  $\mu$  is the system's displacement ductility factor.  $SS_a$  larger than 1.0 indicates an average spectral ordinate that increases with increasing period, and  $SS_a$  smaller than 1.0 indicates an average spectral ordinate that decreases with increasing period.

For  $\mu$  equal to 8, Figure 7 shows  $SS_a$  values computed for periods ranging from 0.1s to 5s. At low periods, no trend is apparent between  $SS_a$  and  $Z_{2.5}$ . In contrast, at longer periods (0.5 to 4s) the Yufutsu recordings have larger median  $SS_a$  values with respect to  $Z_{2.5}$ .

For comparative purposes,  $SS_a$  values for a well-studied crustal set of ground motions are shown. This set of motions were compiled by Haselton et al. [13], consists of 39 record pairs of earthquakes with  $M_w$  ranging from 6.5 to 7.6 earthquakes, were recorded at moderate source-to-site distances (10-45km), and were located on sites with  $V_{S30}$  more than 180 m/s. This set is an expanded version of the far-field ground motion set used in FEMA P695 [37] and in this paper is referred to as the FEMA ground motion set. The median  $SS_a$  values with respect to period for recordings in the FEMA set are shown in Figure 7. For all the bins, the Tokachi-Oki motions have larger values of  $SS_a$  (more damaging) than the FEMA set.

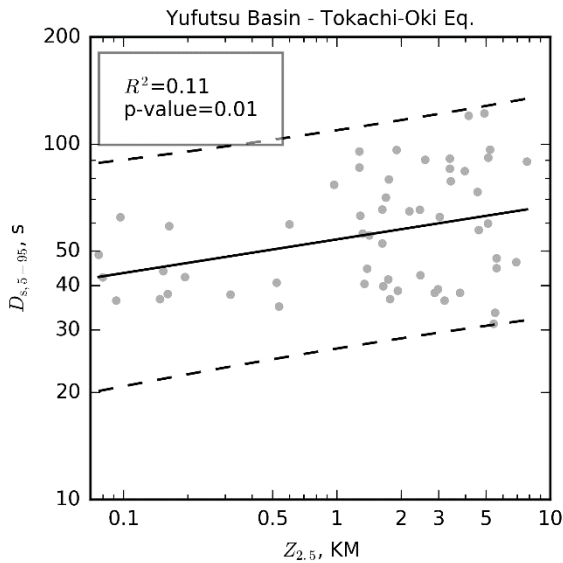


Figure 6. Significant duration with respect to  $Z_{2.5}$

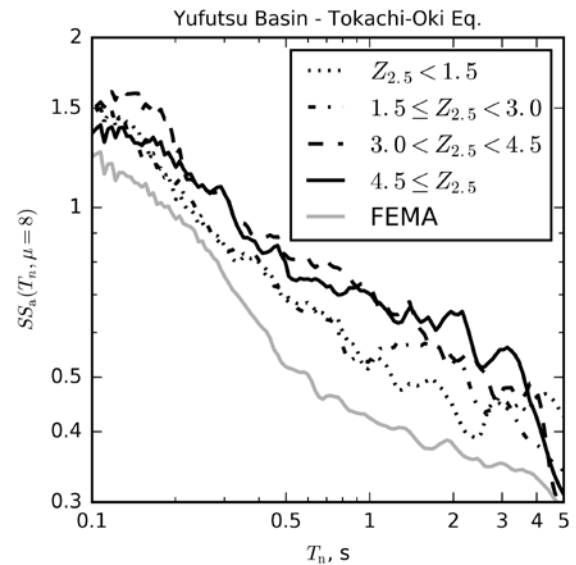


Figure 7. Median of  $SS_a$  with respect to the fundamental period of the structure for various  $Z_{2.5}$  bins

## 7 Effects of Basin on Structural Collapse

To evaluate the effects of basins on structural collapse, dynamic collapse analyses were performed for 30 MDOF archetypical reinforced concrete special moment frame buildings, developed by Haselton et al. [13]. These models were subjected to the inside ( $Z_{2.5} \geq 3$ ) and outside ( $Z_{2.5} < 1.5$ ) Yufutsu basin recordings, and also, to the FEMA set, described earlier. As an example, the collapse fragility functions for each ground-motion set is shown

in Figure 8 for archetype 1022. The median collapse spectral acceleration ( $S_{a,c}$ ) was 0.77g for the inside Yufutsu basin set, 0.95g for the outside basin set, and 1.11g for the FEMA set.

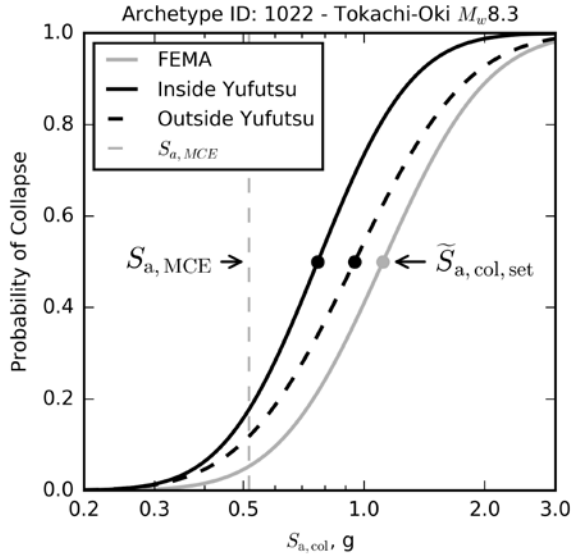


Figure 8. Collapse fragility functions for three ground-motion sets computed using spectral acceleration

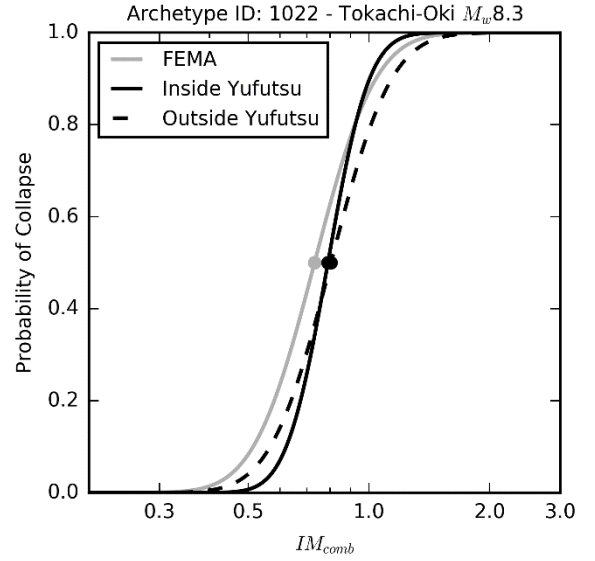


Figure 9. Collapse fragility functions for three ground-motion sets computed using  $IM_{comb}$

These results differ, because structural collapse depends not only on  $S_a$ , but also on other ground-motion characteristics, such as duration and spectral shape. The results show that, at a given level of spectral acceleration, (1) the FEMA are the least likely to cause collapse, (2) the outside basin motions are more damaging than the FEMA ones, and (3) the inside basin motions are the most damaging. These effects can be taken into account by the Marafi et al. [12] intensity measure, which combines spectral acceleration at the period of a structure, significant duration, and  $SS_a$ . The combined IM is computed as,

$$IM_{comb} = S_a(T_n) \times D_{s,5-95\%}^{C_{dur}} \times SS_a^{C_{shape}} \quad \text{Eq. 7}$$

where the empirical exponent  $C_{dur}$  accounts for the structure's sensitivity to  $D_{s,5-95\%}$ , and the  $C_{shape}$  exponent accounts for its sensitivity to  $SS_a$ . These exponents have been previously optimized in [12], where  $C_{dur}$  and  $C_{shape}$  are equal to 0.11 and 0.72 for ductile structures. Figure 9 shows the collapse fragility curves computed using  $IM_{comb}$ . In this calculation, the  $SS_a$  intensity measure was computed with a  $\mu$  equal to 8 quantifying the spectral shape between the period range of  $T_1$  to  $3.68T_1$ , where  $T_1$  is the first-mode period of the structure. The fragility curves computed using  $IM_{comb}$  values are now similar for the three datasets. The new intensity measure also decreases the coefficient of variation computed in log scale for each dataset.

## 7.1 Collapse Margin Ratios

The FEMA P695 guidelines [37] characterizes collapse safety of structures under the maximum considered earthquake in terms of the collapse margin ratio (CMR). The collapse margin ratio for a set of motions,  $CMR_{set}$ , is defined as,

$$CMR_{set} = \frac{\tilde{S}_{a,c,set}}{S_{MT}} \quad \text{Eq. 8}$$

where the  $\tilde{S}_{a,c,set}$  is the median  $S_a$  at collapse for a given ground motion set and  $S_{MT}$  is the spectral acceleration of the maximum considered earthquake at the fundamental period of the structure. The 30 archetypal moment

frames were designed for a short period MCE  $S_a$  equal to 1.5g and a 1-sec MCE  $S_a$  equal to 0.9g. The  $S_{MT}$  for each structure was computed using the design response spectrum defined in FEMA P695 [37].

Figure 8 shows collapse margin ratios for all 30 frames with respect to the building's period for the ground-motion sets. The  $CMR_{inside}$  is smaller than  $CMR_{outside}$  for nearly all (29/30) structures, indicating that inside basin motions are more damaging (attributable to duration and spectral shape). In addition,  $CMR_{inside}$  is smaller than  $CMR_{FEMA}$  for all 30 structures, indicating that the FEMA are least damaging for a particular level of spectral acceleration.

## 7.2 Compensating with Design Factors

Ideally, a structure of the same configuration (similar structural system, seismic mass, number of stories, story height, etc.) would be designed inside and outside the basin to have the same CMRs, i.e.  $CMR_{inside} \approx CMR_{outside}$ . To compare these CMRs, it is necessary to consider: (1) the amplification of spectral acceleration ( $BAF_{S_a}$ ) in the basin, and (2) the reduction of  $\tilde{S}_{a,c}$  between inside to outside basins motions. These effects could be compensated for by amplifying the strength of structures located inside the basin so that their collapse margin ratios would be similar to that of structures outside the basin. This design factor can be expressed as,

$$DF_{outside-inside} = BAF_{S_a} \times \frac{\tilde{S}_{a,c,outside}}{\tilde{S}_{a,c,inside}} \quad \text{Eq. 9}$$

where the  $BAF_{S_a}$  values are obtained from Figure 5 and account for the increase in  $S_{MT}$  due to basin effects. The ratio of the two values of  $\tilde{S}_{a,c}$  accounts for the differences in ground-motion duration and spectral shape, which affect the spectral acceleration at collapse. This design factor assumes that increasing the design force, would proportionally increase the collapse strength and the collapse margin ratios. This might not be correct, if an increase in minimum design strength significantly alters the dynamic properties of the structure. Figure 11 shows the  $DF_{outside-inside}$  values with respect to period for all 30 archetypes. The median  $DF_{outside-inside}$  is 2.2.

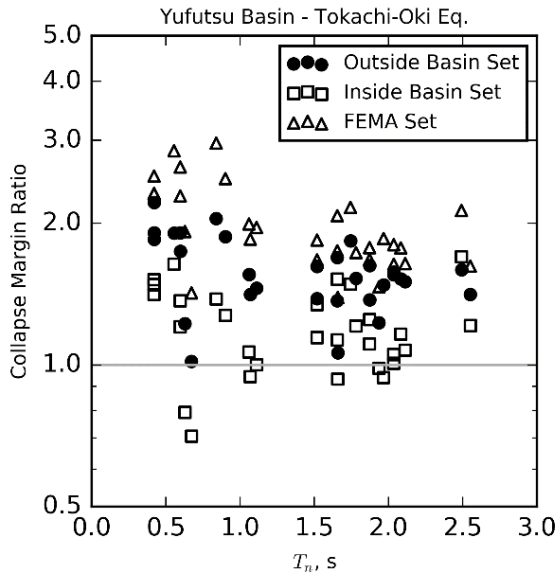


Figure 10. Collapse margin ratios for 30 building archetypes

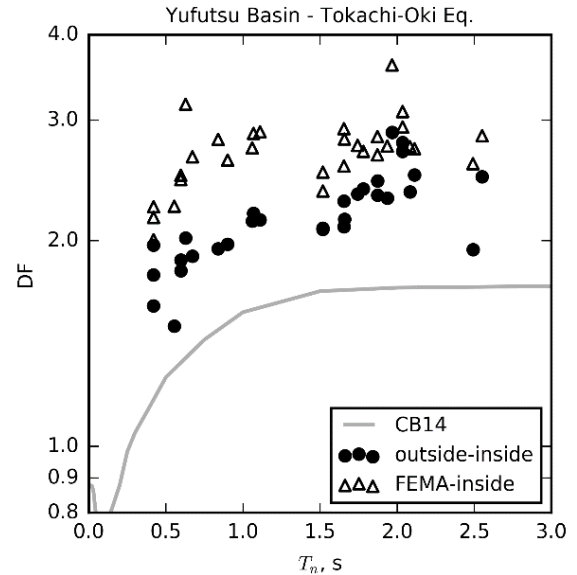


Figure 11. Design factors with respect to period for 30 archetypal frames.

Most structural systems evaluated using the FEMA P695 methodology use the FEMA ground motion set. DF factors relative to the FEMA CMRs can be computed as,

$$DF_{FEMA-inside} = BAF_{S_a} \times \frac{\bar{S}_{a,c,FEMA}}{\bar{S}_{a,c,inside}} \quad \text{Eq. 10}$$

where the  $BAF_{S_a}$  values are obtained from Figure 5. The  $DF_{FEMA-inside}$  expresses the amplification needed that ensure consistent CMRs between structures located inside the Yufutsu basin to crustal earthquakes part of the FEMA set. Figure 11 also shows the  $DF_{FEMA-inside}$  values with respect to period for all 30 archetypes. The median  $DF_{FEMA-inside}$  is 2.7, which is larger than the 2.2 value for  $DF_{outside-inside}$ . Note that these design factors are computed for the situation in which the entire hazard is attributable to subduction earthquakes. In reality, the appropriate design factor might be lower if other earthquake types contributed significantly to the seismic hazard at a location.

### 7.3 Comparison with CB 14

Recently, Chang et al. [25] developed tall building design recommendations for Puget Sound. These recommendations account for basin effects by amplifying the  $S_a$  in the hazard response spectrum using the CB14 basin term. To compare  $DF_{outside-inside}$  and  $DF_{FEMA-inside}$  values with CB14,  $DF_{CB14}$  design factors are computed as,

$$DF_{CB14} = \exp \frac{f_{basin}(\tilde{Z}_{2.5,inside})}{f_{basin}(\tilde{Z}_{2.5,outside})} \quad \text{Eq. 11}$$

where  $f_{basin}$  is the basin term (in log-scale) in CB14 and  $\tilde{Z}_{2.5,inside}$  is the median  $Z_{2.5}$  for inside basin records and  $\tilde{Z}_{2.5,outside}$  is the median  $Z_{2.5}$  for outside basin recordings. Figure 11 shows  $DF_{CB14}$  are smaller than both  $DF_{outside-inside}$  and  $DF_{FEMA-inside}$  for all structures. Assuming that the Yufutsu basin and Puget Lowlands have similar characteristics, these results suggest that the CB14 basin amplification term does not result in similar CMRs between structures inside and outside basins.

## 8 Conclusions

The effects of the Yufutsu basin during the Tokachi-Oki earthquake are evaluated in terms of the spectral acceleration, significant duration, and a spectral shape intensity measure,  $SS_a$ . Collapse analyses were performed for 30 archetypical concrete moment frame structures to evaluate their margin of safety against collapse during subduction earthquakes inside and outside of the basin.

Spectral accelerations correlated well with the basin depth measure,  $Z_{2.5}$ . The variability of  $S_a$  due to local site effects was accounted for with the GMPE residuals. The resulting basin amplification factors for  $S_a$  generally increased with period, reaching maximum values between 2 to 3 at long periods (5-7s).  $BAF_{S_a}$  were found to be insensitive to magnitude. Significant duration was found to correlate weakly with basin depth. However, spectral shape (measured using  $SS_a$ ) was shown to be larger (and consequently, more damaging) inside the Yufutsu basin for periods between 0.5-4s and more damaging than the FEMA set for nearly all periods and all basin depths.

Collapse margin ratios computed with inside Yufutsu basin motions were nearly always smaller than outside Yufutsu basin motions and FEMA motions. The differences in CMRs, attributable to differences in ground-motion duration and spectral shape, could be reconciled by expressing the collapse ground-motion intensity in terms of  $IM_{comb}$ .

Design strength amplification factors on the structure's yield strength were computed to ensure consistent collapse margin ratio between structures located inside and outside the basin. These design factors (ranging from about 2 to 3) account for differences in spectral acceleration, duration, and spectral shape. These design factors for all structures were found to be larger than the basin factors computed using CB14.

## 9 Acknowledgements

The authors would like to thank Curt Haselton for sharing 30 RC SMF building models. The authors appreciate input from Erin Wirth and Arthur Frankel throughout the development of this paper. This research was funded

by the National Science Foundation under award number EAR-1331412. The computations were facilitated through the use of advanced computational, storage, and networking infrastructure provided by the Hyak supercomputer system at the University of Washington.

## 10 References

- [1] Kawase H (1996): The Cause of the Damage Belt in Kobe: “The Basin-Edge Effect,” Constructive Interference of the Direct S-Wave with the Basin-Induced Diffracted/Rayleigh Waves. *Seismological Research Letters*; **67**(5): 25–34. DOI: 10.1785/gssrl.67.5.25.
- [2] Graves RW, Pitarka A, Somerville PG (1998): Ground-motion amplification in the Santa Monica area: Effects of shallow basin-edge structure. *Bulletin of the Seismological Society of America*; **88**(5): 1224–1242.
- [3] Hatayama K, Kanno T, Kudo K (2007): Control Factors of Spatial Variation of Long-Period Strong Ground Motions in the Yufutsu Sedimentary Basin, Hokkaido, during the Mw 8.0 2003 Tokachi-oki, Japan, Earthquake. *Bulletin of the Seismological Society of America*; **97**(4): 1308–1323. DOI: 10.1785/0120060200.
- [4] Frankel A, Stephenson W, Carver D (2009): Sedimentary Basin Effects in Seattle, Washington: Ground-Motion Observations and 3D Simulations. *Bulletin of the Seismological Society of America* 2009; **99**(3): 1579–1611. DOI: 10.1785/0120080203.
- [5] Choi Y, Stewart JP, Graves RW (2005): Empirical Model for Basin Effects Accounts for Basin Depth and Source Location. *Bulletin of the Seismological Society of America*; **95**(4): 1412–1427. DOI: 10.1785/0120040208.
- [6] Heaton T, Yang J, Hall J (2006): Simulated performance of steel moment-resisting frame buildings in the 2003 Tokachi-oki earthquake. *Bulletin of the Earthquake Research Institute*, 81 (3-4). pp. 325-329. ISSN 0040-8972.
- [7] USGS (United States Geological Survey) (2008): Interactive Deaggregations. <<http://geohazards.usgs.gov/deaggint/2008/>> [accessed May 5, 2016].
- [8] Bommer JJ, Magenes G, Hancock J, Penazzo P (2004): The influence of strong-motion duration on the seismic response of masonry structures. *Bulletin of Earthquake Engineering*; **2**(1):1-26. DOI: 10.1023/B:BEEE.0000038948.95616.bf
- [9] Hancock J and Bommer JJ (2007): Using spectral matched records to explore the influence of strong-motion duration on inelastic structural response. *Soil Dynamics & Earthquake Engineering*; **27**(4):291-299. DOI: 10.1016/j.soildyn.2006.09.004
- [10] Chandramohan R, Baker JW, Deierlein GG (2015): Quantifying the influence of ground motion duration on structural collapse capacity using spectrally equivalent records. *Earthquake Spectra*; In-Press.
- [11] Raghunandan M, Liel AB (2013): Effect of ground motion duration on earthquake-induced structural collapse. *Structural Safety*; **41**:119–133. DOI:10.1016/j.strusafe.2012.12.002.
- [12] Marafi NA, Berman JW, Eberhard MO (2016): Ductility-dependent intensity measure that accounts for ground-motion spectral shape and duration. *Earthquake Engng Struct. Dyn.*, 45: 653–672. doi: 10.1002/eqe.2678.
- [13] Haselton CB, Liel AB, Deierlein GG, Dean BS, Chou JH (2011) Seismic Collapse Safety of Reinforced Concrete Buildings. I: Assessment of Ductile Moment Frames. *Journal of Structural Engineering*; **137**(4):481–491. DOI: 10.1061/(ASCE)ST.1943-541X.0000318.
- [14] Petersen MD, Moschetti MP, Powers PM, Mueller CS, Haller KM, Frankel AD, Zeng Y, Rezaeian S, Harmsen SC, Boyd OS, Field N, Chen R, Rukstales KS, Luco N, Wheeler RL, Williams RA, Olsen AH (2014): Documentation for the 2014 update of the United States national seismic hazard maps: U.S. Geological Survey Open-File Report 2014–1091, 243 p., <http://dx.doi.org/10.3133/ofr20141091>
- [15] ASCE (2013): *Minimum design loads for buildings and other structures*, Standard ASCE/SEI 7-10. American Society of Civil Engineers (ASCE): Reston, Virginia.
- [16] Abrahamson NA, Silva WJ, Kamai R (2014): Summary of the ASK14 Ground Motion Relation for Active Crustal Regions. *Earthquake Spectra*; **30**(3): 1025–1055. DOI: 10.1193/070913EQS198M.
- [17] Boore DM, Stewart JP, Seyhan E, Atkinson GM (2014): NGA-West2 Equations for Predicting PGA, PGV, and 5% Damped PSA for Shallow Crustal Earthquakes. *Earthquake Spectra*; **30**(3): 1057–1085. DOI: 10.1193/070113EQS184M.
- [18] Chiou BJS, Youngs RR (2014): Update of the Chiou and Youngs NGA Model for the Average Horizontal Component of Peak Ground Motion and Response Spectra. *Earthquake Spectra*; **30**(3): 1117–1153. DOI: 10.1193/072813EQS219M.
- [19] Campbell KW, Bozorgnia Y (2014): NGA-West2 Ground Motion Model for the Average Horizontal Components of PGA, PGV, and 5% Damped Linear Acceleration Response Spectra. *Earthquake Spectra*; **30**(3): 1087–1115. DOI: 10.1193/062913EQS175M.
- [20] Atkinson GM, Boore DM (2003): Empirical Ground-Motion Relations for Subduction-Zone Earthquakes and Their

- Application to Cascadia and Other Regions. *Bulletin of the Seismological Society of America*; **93**(4): 1703–1729. DOI: 10.1785/0120020156.
- [21] Zhao JX (2006): Attenuation Relations of Strong Ground Motion in Japan Using Site Classification Based on Predominant Period. *Bulletin of the Seismological Society of America*; **96**(3): 898–913. DOI: 10.1785/0120050122.
- [22] Atkinson GM, Macias M (2009): Predicted Ground Motions for Great Interface Earthquakes in the Cascadia Subduction Zone. *Bulletin of the Seismological Society of America*; **99**(3): 1552–1578. DOI: 10.1785/0120080147.
- [23] Addo, Kofi, Abrahamson, Norman, and Youngs, Robert (2012): (BC Hydro), 2012, Probabilistic seismic hazard analysis (PSHA) model—Ground motion characterization (GMC) model: Report E658, published by BC Hydro.
- [24] Morikawa N, Fujiwara H (2013): A New Ground Motion Prediction Equation for Japan Applicable up to M9 Mega-Earthquake. *Journal of Disaster Research*; **8**(5): 878–888. DOI: 10.20965/jdr.2013.p0878.
- [25] Chang SW, Frankel AD, Weaver CS (2014): Report on Workshop to Incorporate Basin Response in the Design of Tall Buildings in the Puget Sound region, Washington: U.S. Geological Survey, Open-File Report 2014–1196, 28 p. DOI: <http://dx.doi.org/10.3133/ofr20141196>.
- [26] Haselton CB, Baker JW, Liel AB, Deierlein GG (2011): Accounting for Ground-Motion Spectral Shape Characteristics in Structural Collapse Assessment through an Adjustment for Epsilon. *Journal of Structural Engineering*; **137**(3):332–344. DOI:10.1061/(ASCE)ST.1943-541X.0000103.
- [27] Eads L, Miranda E, Lignos DG (2015): Average spectral acceleration as an intensity measure for collapse risk assessment. *Earthquake Engineering & Structural Dynamics*; **44**(12):1899-2135. DOI:10.1002/eqe.2575.
- [28] Koketsu K, Miyake H, Afnimar, Tanaka Y (2009): A proposal for a standard procedure of modeling 3-D velocity structures and its application to the Tokyo metropolitan area, Japan. *Tectonophysics*; **472**(1-4): 290–300. DOI: 10.1016/j.tecto.2008.05.037.
- [29] Blakely RJ, Wells RE, Weaver CS, Johnson SY (2002): Location, structure, and seismicity of the Seattle fault zone, Washington: Evidence from aeromagnetic anomalies, geologic mapping, and seismic-reflection data. *Geological Society of America Bulletin*; **114**(2): 169–177. DOI: 10.1130/0016-7606(2002)114<0169:LSASOT>2.0.CO;2.
- [30] K-NET, KiK-net (2016): Strong-motion seismograph networks, <<http://www.kyoshin.bosai.go.jp/>> (Apr. 21, 2016)
- [31] Boore DM, Thompson EM, Cadet H (2011): Regional Correlations of VS30 and Velocities Averaged Over Depths Less Than and Greater Than 30 Meters. *Bulletin of the Seismological Society of America*; **101**(6): 3046–3059. DOI: 10.1785/0120110071.
- [32] USGS (2016): ShakeMap, United State Geological Survey Shake Map. <<http://earthquake.usgs.gov/earthquakes/shakemap/>> (Apr. 21, 2016)
- [33] Abrahamson N, Gregor N, Addo K (2016): BC Hydro Ground Motion Prediction Equations for Subduction Earthquakes. *Earthquake Spectra*; **32**(1): 23–44. DOI: 10.1193/051712EQS188MR.
- [34] Abrahamson NA, Silva WJ (1996): Empirical ground motion models. Technical Report, Report to Brookhaven National Laboratory, Upton, NY.
- [35] Kempton JJ, Stewart JP. Prediction Equations for Significant Duration of Earthquake Ground Motions Considering Site and Near-Source Effects. *Earthquake Spectra* 2006; **22**(4): 985–1013. DOI: 10.1193/1.2358175.
- [36] Bommer JJ, Stafford PJ, Alarcon JE (2009): Empirical Equations for the Prediction of the Significant, Bracketed, and Uniform Duration of Earthquake Ground Motion. *Bulletin of the Seismological Society of America* 2009; **99**(6): 3217–3233. DOI: 10.1785/0120080298.
- [37] FEMA (Federal Emergency Management Agency) (2009): *Quantification of Building Seismic Performance Factors*. FEMA P695, Redwood, CA. 2009.